

Programmable Multimode Quantum Networks

Seiji Armstrong^{1,2,3}, Jean-François Morizur^{1,4}, Jiri Janousek^{1,2}, Boris Hage^{1,2}, Nicolas Treps⁴, Ping Koy Lam² and Hans-A. Bachor¹

¹ARC Centre of Excellence for Quantum-Atom Optics,

The Australian National University, Canberra, ACT 0200, Australia

²Centre for Quantum Computation and Communication Technology,

Department of Quantum Science, The Australian National University, Canberra, ACT 0200, Australia

³Department of Applied Physics, School of Engineering,

The University of Tokyo, 7-3-1 Hongo, Bunkyo-ku, Tokyo 113-8656, Japan

⁴Laboratoire Kastler Brossel, Université Pierre et Marie Curie Paris 6, ENS, CNRS, Paris, France

Entanglement between large numbers of quantum modes¹ is the quintessential resource for quantum information processing^{2,3} and future applications such as the quantum internet⁴. Conventionally the generation of multimode entanglement in optics requires complex layouts of beam-splitters and phase shifters in order to transform the input modes in to entangled modes. These networks need substantial modification for every new set of entangled modes to be generated. Further, the complexity grows rapidly with the number of entangled modes as the number of detectors, phase locks and optical components needs to be increased. Here we report on the highly efficient and versatile generation of various multimode entangled states within one optical beam. By defining our modes to be combinations of different spatial regions of the beam, we may use just one pair of multi-pixel detectors and one local oscillator to measure an orthogonal set of modes. The transformation of this set into a desired set of entangled modes is calculated ahead of time via a programmable virtual network of beam-splitters and phase shifters. The transformation is then applied during detection in real time. This enables us to change the set of measured entangled modes via software only, optimizing the network for the desired outputs without modifying the optical setup. The virtual networks are fully equivalent to the physical linear optics networks they are emulating. We show that up to N-mode entanglement is measurable given just one pair of detectors each with N photodiodes, and demonstrate N=2 up to N=8 modes here. Our approach introduces flexibility and scalability to multimode entanglement, two important attributes that are presently lacking in state of the art devices.

In optics, several impressive demonstrations of multipartite entanglement have been shown recently including a 6-photon cluster state⁵ and a 9-mode state used for error correction⁶. However, these schemes tend to employ one detection system per entangled mode/qubit, which introduces a lack of flexibility and is detrimental to its

scalability. These optical setups are built to produce one set of outputs or to perform one given protocol; in order to change the output the optical hardware itself must be modified. We report here on a system with the ability to switch in real time between desired output states using just one detection scheme.

Currently the well-established recipe for generating entanglement using continuous wave laser beams is to mix squeezed modes of light together at beam-splitters. It is possible to create N-mode entanglement given a network of N-1 beam-splitters with N input modes, even with less than N squeezed modes⁷. In our scheme we co-propagate all possible spatial modes of light within one beam. Entanglement between co-propagating modes in one beam has been previously demonstrated with spatial modes⁸, and also in the frequency domain⁹. In the current work we extend the idea of one-beam entanglement by introducing the notion of emulating linear optics networks, by programming virtual networks that mix together different spatial regions of the detected light beam. These software based networks calculate the precise weighted combinations of the spatial regions required to emulate the physical networks. Figure 1 shows two such networks which produce a 2-mode entangled state and an 8-mode entangled state respectively. We also program virtual networks for 3, 4, 5, 6, and 7-mode entangled states, the results of which are shown in Table 1 and Figure 5. By employing custom made multi-photodiode-homodyne-detectors (MPHD) that each contain an array of 8 photodiodes (see Figure 2) we detect the light in 8 spatial regions and assign individual electronic gains to each spatial region. The linear combination of the 8 gain-adjusted photocurrents constitutes the measurement of a mode, \hat{a} :

$$\hat{a} = \sum_{p=1}^8 el_p \hat{i}_p \quad (1)$$

where \hat{i}_p is the homodyne subtracted photocurrent operator at photodiode p , and el_p is the electronic gain applied at p . The n th mode \hat{a}_n for $1 \leq n \leq N$ is uniquely defined by the gain vector G_n containing the 8 electronic gain values el_p^n such that $G_n = [el_1^n \quad el_2^n \quad \dots \quad el_8^n]$. Therefore each spatial mode we measure is defined by a unique

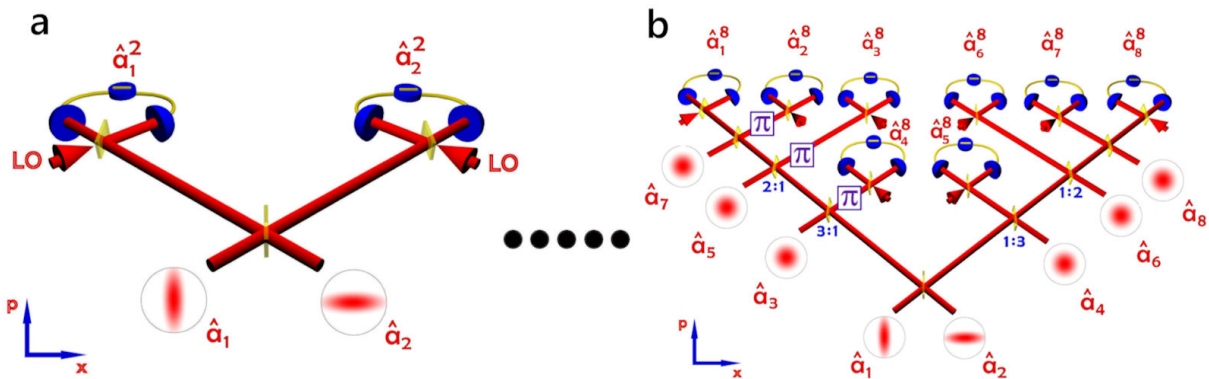


FIG. 1: Multimode entanglement via emulated linear optics networks. Squeezed light and vacua are mixed together using unitary operations in order to produce entangled mode states. Unless otherwise stated beam-splitters are 50% reflective. Superscripts denote mode basis and subscripts denote mode number. **a**, The emulated linear optics network used to measure 2-mode EPR entanglement. **b**, 8-mode entanglement via a calculated concatenation of beam-splitter and π phase shift operations. The dots between **a** and **b** imply virtual networks for $N = 3 \dots 7$, not shown here for brevity (results shown in Figure 5).

pattern within the light beam. These spatial mode patterns, Gaussian profiles modulated by respective electronic gains, are shown visually in Figure 3, while the detection stage of Figure 2 shows how we implement this experimentally. The spatial modes are orthogonal to each other, spanning a basis so that the independent measurement of each mode is possible¹⁰.

We create two amplitude squeezed modes via optical parametric amplification (OPA). The first mode is converted to a flip mode (FM) by phase delaying half its beam by half a wavelength, π (see inset of Fig. 2). The FM is overlapped in quadrature with the Gaussian mode (GM) output of the second OPA upon reflection of its output coupler¹¹. These two squeezed modes are the first two modes of what we refer to as the input basis; \hat{a}_1 and \hat{a}_2 . Six co-propagating vacua modes are measured by calculating G_n vectors that are orthogonal to both \hat{a}_1 and \hat{a}_2 . These vacua modes (labeled $\hat{a}_3 \dots \hat{a}_8$) complete the input mode basis (see middle row of Figure 3). Each spatial mode is characterised by the quadrature operators \hat{x} and \hat{p} of the electric field operator. The \hat{x} and \hat{p} variance measurements of the eight modes in the input basis are shown in Fig. 5 (**a** and **b**). Here, $\langle [\Delta x_{GM}]^2 \rangle = \langle [\Delta x_1]^2 \rangle = -4.3 \pm 0.05\text{dB}$ and $\langle [\Delta x_{FM}]^2 \rangle = \langle [\Delta x_2]^2 \rangle = -3.7 \pm 0.05\text{dB}$ below the standard quantum noise, and the variances of the vacua are verified to equal quantum noise.

A basis of entangled modes is measured by taking N modes from the input mode basis and mixing them together in a linear combination calculated by virtual networks. After a calibration run to measure the input mode basis, optimal virtual networks are calculated allowing for optimisation of beam-splitters due to asymmetries in the squeezing levels of input modes. The unitaries we have access to in programming the virtual networks are

beam-splitters and π phase shifts. The π phase shift is equivalent to multiplying \hat{a} by -1 . Note that arbitrary phase shifts are forbidden as each measurement naturally corresponds to detection at a fixed phase defined by a shared reference beam, the local oscillator. Importantly, each of these virtual network mappings are stored offline, to be used at the time of detection to project the MPHD subtracted photocurrent onto any desired basis in real time. Linear optics networks are emulated by this unique mapping from the input mode basis to an entangled mode basis.

The most intuitive virtual network we create is the 2-mode EPR state¹² shown in Figure 1 (a) with 2 squeezed inputs. Here we engineer spatial mode patterns which have no spatial overlap; the left half of the beam is entangled with the right half (see the top left of Figure 3). Spatial Modes measured in a mode basis are given a superscript N to distinguish them from modes in the input basis; a_1^2 and a_2^2 represent the two modes spanning the $N=2$ -mode EPR basis. The supplementary methods detail how we create virtual networks for each of the $N=2, 3, 4, 5, 6, 7$, and 8-mode bases. In general we construct networks pertaining to N modes by concatenating $N-1$ virtual beam-splitters with vacua on unused input ports. This is a highly efficient approach to creating multimode entanglement as the arduous tasks of mode matching and alignment are replaced with the ease of programming.

In order to verify entanglement between measured modes we use the well-established van Loock-Furusawa inseparability criteria¹³. For an N -mode entangled state,

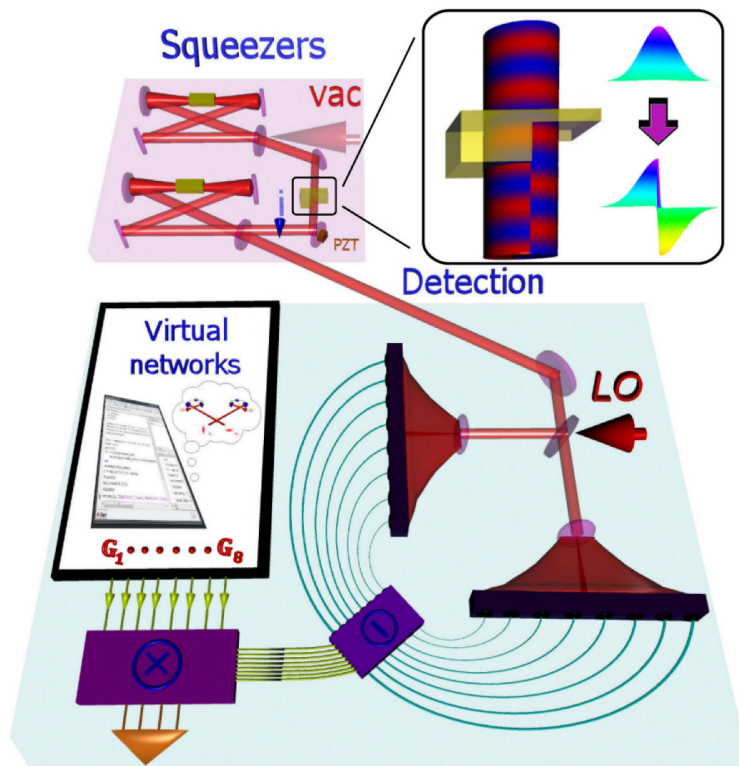


FIG. 2: Experimental setup. (not to scale). Squeezed light is prepared and combined in *squeezers* with a piezo electric transducer (PZT) controlling the phase between the two squeezed modes, locked in quadrature. Vacuum modes (*vac*) co-propagate so that the beam exiting *squeezers* and entering *detection* contains 8 measurable spatial modes. Multi-pixel homodyne detection (MPHD) is used to measure the quadrature amplitudes of the beam in 8 different regions, in *detection*. Local oscillator (LO) gives a reference to phase quadratures. A PC is used to calculate electronic gain functions G_n via the notion of *virtual networks*. The detected beam is then projected onto a basis of measured modes (see equation 1). **(Inset)** Flip mode (FM) generation; half of the wave is phase retarded by half a wavelength, flipping the electric field amplitude.

it is sufficient to satisfy $N - 1$ inseparability inequalities:

$$\begin{aligned}
 & \text{(I)} \\
 & \langle [\Delta(\hat{x}_1 - \hat{x}_2)]^2 \rangle \\
 & + \langle [\Delta(\hat{p}_1 + \hat{p}_2 + g_3\hat{p}_3 + \dots + g_N\hat{p}_N)]^2 \rangle < 1, \\
 & \dots \\
 & \dots \\
 & \text{(N-1)} \\
 & \langle [\Delta(\hat{x}_{N-1} - \hat{x}_N)]^2 \rangle \\
 & + \langle [\Delta(g_1\hat{p}_1 + \dots + g_{N-2}\hat{p}_{N-2} + \hat{p}_{N-1} + \hat{p}_N)]^2 \rangle < 1.
 \end{aligned} \tag{2}$$

with free parameters g_i , to be optimised for maximum inseparability. We have omitted the superscript N here for clarity, as the above holds for any mode basis. The subscripts n of \hat{x} and \hat{p} here indicate the n th mode in the N -mode basis. Table I summarises the measured degrees of inseparability for all $N - 1$ inequalities in each N -mode basis, given in roman numerals.

The terms in equation (2) measure the degree of correlations between any two modes in a given basis. The L.H.S. of equation (2) contains the sum of two correlation variances; correlations in the x quadrature and anti-correlations in the p quadrature. For the modes to be inseparable, each of these correlation variances must

be in the quantum regime, that is below the normalised quantum noise of two units of vacua. Figure 5 (c, d) shows this to be the case in our experimental measurements. Even without increasing the number of squeezing resources, this scheme is scalable to higher numbers of mode entanglement, as shown in Figure 5 (e). As we increase the number of modes in the basis up to 20, the degree of inseparability approaches the classical bound of 1 due to the vacuum noise penalty for each additional unsqueezed mode input. Entanglement is shown to hold here however, even with current squeezing levels. Importantly, there is no loss incurred during the transformation of the squeezed input modes into a set of entangled modes, as can be seen by the agreement of the theoretical predictions and the experimental values of Figure 5 (e). This equates to perfect mode matching at every virtual beam-splitter. Figure (S-5) of the supplementary material explores how inseparability scales with different squeezing levels. Measuring a larger number of modes experimentally requires only an increase in the number of photodiodes in the MPHD, and importantly no modification of the optical setup.

For the special case of $N = 2$, EPR entanglement¹⁴

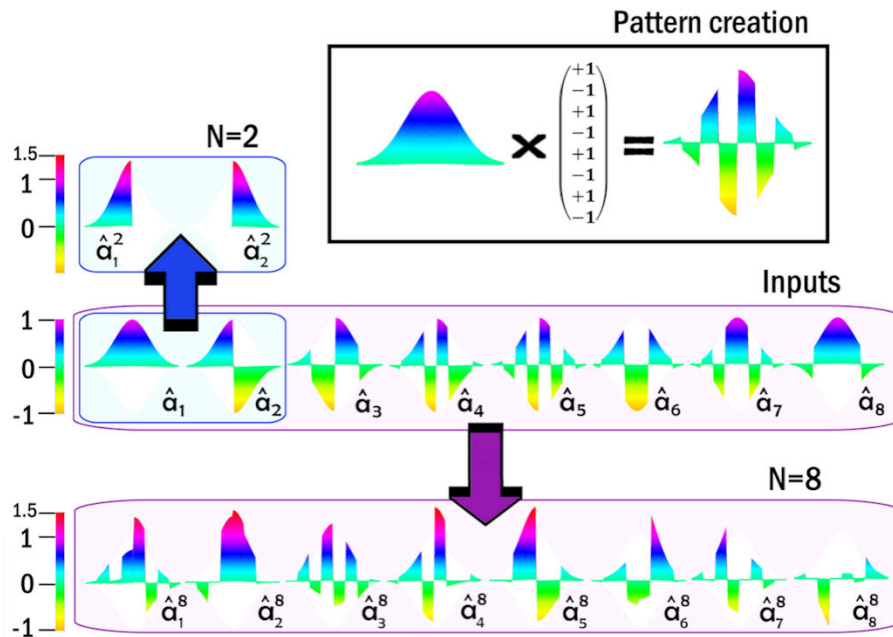


FIG. 3: Spatial mode patterns. Measured modes are defined by spatial patterns of electric field amplitudes. Shown in the *pattern creation* box is an example of how the spatial mode pattern for \hat{a}_5 is created by following equation (1) and applying 8 electronic gain values (G_n) to the detected light. The basis of input modes $\hat{a}_1 \dots \hat{a}_8$ is shown on the middle row. The arrows represent a mapping via virtual networks onto bases of entangled quantum modes (modes). The top row shows the EPR or 2-mode basis, while the bottom row shows the 8-mode basis. There is a one-to-one correspondence between spatial mode bases shown here ($\{\hat{a}_i\}, \{\hat{a}_i^2\}, \{\hat{a}_i^8\}$) and those shown in Figure 1. Again, spatial mode bases for $N=3$ to $N=7$ not shown for brevity.

is measured to be 0.59 ± 0.01 . Optimising for the beam-splitter reflectivity¹⁵ we find that due to the asymmetry between input squeezing levels, the optimal beam-splitter ratio here is not 50%, but rather 48.8%. Each unique beam-splitter reflectivity changes the mapping to a new basis, so the beam of light contains an infinite number of mode bases. The versatility of our scheme comes from having access to this plethora of mode bases, allowing us to measure the output modes corresponding to an optimal network given an arbitrary set of asymmetric inputs.

The entanglement demonstrated in the current work allows for such protocols as quantum teleportation^{16,17,7}. To perform complex protocols such as one-way measurement based quantum computations² modifications are needed. The resource states needed, cluster states^{18,19}, may be created with the current setup by simply increasing the squeezing resources. To perform computations on the cluster states however we need access to arbitrary homodyne angles of each mode, and the ability to perform feed-forward to any desired mode²⁰. Both are feasible with existing technologies^{21–23}.

Emulating linear optics networks by mixing copropagating spatial modes is a highly efficient method for generating multimode entanglement. Otherwise arduous and potentially lossy tasks such as mode matching during the construction of a linear optics network are performed effortlessly and losslessly via software

controlled combinations of the spatial modes. We have shown that although correlations weaken if more squeezing resources are not added, entangled modes scale here as the number of orthogonal modes measurable within the beam. This corresponds directly to the number of photodiodes in each pair of the multi-pixel detectors. We have demonstrated this by measuring $N=2, 3, 4, 5, 6, 7,$ and 8-mode entanglement within one beam, switching between them in real time. The ability to perform a wide range of protocols and optimise networks for asymmetry using just one optical setup offers versatility to future networks that will utilise entanglement as a resource.

-
- [1] Furusawa, A., van Loock, P. *Quantum Teleportation and Entanglement* (Wiley-VCH, Weinheim, Germany, 2011).
 - [2] Raussendorf, R., Briegel, H. J. A one-way Quantum Computer. *Phys. Rev. Lett.* **86**, 5188-5191 (2001).
 - [3] Menicucci, N. C. et al. Universal Quantum computation with continuous-variable cluster states. *Phys. Rev. Lett.* **97**, 110501 (2006).
 - [4] Kimble, J. The quantum internet. *Nature* **453**, 1023-1030 (2008).
 - [5] Lu, C-Y. et al. Experimental entanglement of six photons in graph states. *Nature* **3**, 91-95 (2007).

- [6] Aoki, T. et al. Quantum error correction beyond qubits. *Nature Physics* **5**, 541-546 (2009).
- [7] van Loock, P., Braunstein, S. L. Multipartite Entanglement for continuous variables: a quantum teleportation network. *Phys. Rev. Lett.* **84** (15), 3482-3485 (2000).
- [8] Janousek, J. et al. Optical entanglement of co-propagating modes. *Nature Photonics* **3**(7), 399-402 (2009).
- [9] Pysher, M., Miwa, Y., Shahrokhshahi, R., Bloomer, R., Pfister, O. Parallel generation of quadripartite cluster entanglement in the optical frequency comb. *Phys. Rev. Lett* **107**, 030505 (2011).
- [10] Beck, M. Quantum state tomography with array detectors. *Phys. Rev. Lett.* **84** (25), 5748 (2000).
- [11] Delaubert, V. Generation of a phase-flipped Gaussian mode for optical measurements. *J. Opt. A* **4**, 393 (2002).
- [12] Einstein, A., Podolsky, B., Rosen, N. Can quantum-mechanical description of physical reality be considered complete? *Phys. Rev.* **47**, 777 (1935).
- [13] van Loock, P., Furusawa, A. Detecting genuine multipartite continuous-variable entanglement. *Phys. Rev. A.* **67**, 052315 (2003).
- [14] Reid, M.D., Drummond, P.D. Quantum correlations of phase in nondegenerate parametric oscillation. *Phys. Rev. Lett.* **60**, 2731 (1988).
- [15] Bowen, W. P., Lam, P-K., Ralph, T. C. Biased EPR entanglement and its application to teleportation. *J. Mod. Optics* **50**, 801-813 (2003).
- [16] Bennett, C.H. et al. Teleporting an unknown quantum state via dual classical and Einstein-Podolsky-Rosen channels. *Phys. Rev. Lett.* **70**, 1895 (1993).
- [17] Furusawa, A. et al. Unconditional quantum teleportation. *Science* **282** (5389): 706-709 (1998).
- [18] Yukawa, M., Ukai, R., van Loock, P., Furusawa, A. Experimental generation of four-mode continuous-variable cluster states. *Phys. Rev. A* **78**, 012301 (2008).
- [19] Su, X. et al. Experimental preparation of quadripartite cluster and Greenberger-Horne-Zeilinger entangled states for continuous-variables. *Phys. Rev. Lett.* **98**, 070502 (2007).
- [20] Ukai, R. et al. Demonstration of unconditional one-way quantum computations for continuous variables. *Phys. Rev. Lett.* **104**, 240504 (2011).
- [21] Morizur, J-F. et al. Programmable unitary spatial mode manipulation. *JOSA A* **27**, 11 2524-2531 (2010).
- [22] Morizur, J-F., Armstrong, S., Treps, N., Janousek, J., Bachor, H-A. Spatial reshaping of a squeezed state of light. *EPJD* **61**, 1 237-239 (2011).
- [23] Morizur, J-F. *Quantum Protocols with Transverse Spatial Modes*. (PhD thesis, Aust. Nat. Univ., 2011).

Acknowledgements This research was conducted by the Australian Research Council Centre of Excellence for Quantum-Atom Optics (project number CE0348178), in collaboration with the network "High-dimensional entangled systems" (HIDEAS FP7-ICT-221906) funded by the European Union, as well as the Australian Research Council Centre of Excellence for Quantum Computation and Communication Technology (project number CE110001029). The authors thank Akira Furusawa and the Furusawa group for discussions. SA is grateful for funding from the Australia-Asia Prime Minister's Award. BH acknowledges funding from the Alexander von Humboldt foundation.

Author contributions

S.A., J-F.M., J. J., N. T. and H-A. B. designed the experiment. J.J. designed and built both of the optical parametric amplifiers. S.A., J-F.M. and J. J. constructed and performed the experiment. B.H. designed and built the multi-photodiode homodyne detectors, taught S.A. how to code the digital locking system, and designed the software filters used in data analysis. P-K.L. and H-A.B. supervised the experiment. S.A. performed the data analysis and wrote the manuscript. J-F.M. wrote the data acquisition code and provided support in the data analysis.

TABLE I: Inseparability of quantum modes based on the van Loock-Furusawa criteria. Each row shows that for a basis of N quantum modes, the N-1 values obtained from quadrature variances are well below 1. This verifies entanglement of the N quantum modes.

N	I	II	III	IV	V	VI	VII	Avg.
2	0.39							0.39
3	0.56	0.56						0.56
4	0.64	0.63	0.64					0.64
5	0.69	0.69	0.70	0.70				0.69
6	0.73	0.73	0.75	0.74	0.74			0.74
7	0.77	0.78	0.77	0.76	0.77	0.77		0.77
8	0.79	0.79	0.78	0.81	0.79	0.80	0.79	0.79

*Uncertainty is ± 0.01 in all cases.

Supplementary Material

Virtual Networks

The virtual networks are programmed using matrix based software on a standard PC. The networks are concatenations of two important unitary operations: the beam splitter (BS), and the π phase shift. The BS operation $\hat{B}(r)$ acting on inputs $\hat{a}_{1\text{in}}, \hat{a}_{2\text{in}}$, to produce outputs $\hat{a}_{1\text{out}}, \hat{a}_{2\text{out}}$, is defined as follows:

$$\begin{pmatrix} \hat{a}_{1\text{out}} \\ \hat{a}_{2\text{out}} \end{pmatrix} = \begin{pmatrix} \sqrt{r} & \sqrt{t} \\ \sqrt{t} & -\sqrt{r} \end{pmatrix} \begin{pmatrix} \hat{a}_{1\text{in}} \\ \hat{a}_{2\text{in}} \end{pmatrix} \quad (3)$$

where r and t are the reflectivity and transmissivity of the BS, respectively, with $\sqrt{t} = \sqrt{r-1}$. The π phase shift is equivalent to multiplying \hat{a} by -1 . Formally, each spatial mode \hat{a}_n for $1 \leq n \leq N$ is defined as

$$\hat{a}_n = \sum_{p=1}^8 e l_p^n \hat{i}_p \quad (4)$$

where \hat{i}_p is the homodyne subtracted photocurrent operator at photodiode p and $e l_p^n$ is the electronic gain applied at p for the n th mode. For convenience we define a vector G containing 8 electronic gains: $G = [e l_1 \ e l_2 \ \dots \ e l_8]$ such that each vector $G_n = [e l_1^n \ e l_2^n \ \dots \ e l_8^n]$ uniquely projects the photocurrents \hat{i}_p onto the measured mode \hat{a}_n . The orthogonality between measured modes in any basis is verified by showing that the inner product between any two modes \hat{a}_i and \hat{a}_j ($i \neq j$) is zero.

For even numbered mode bases ($N = 2, 4, 6, 8$) the method for creating the virtual network is as follows. The two squeezed modes a_1 and a_2 are combined on a half reflecting beamsplitter (HBS). As the output of this HBS is an EPR state we choose to call this the EBS. The EBS outputs are symmetrically combined with $N - 2$ vacua, as in Figure 1 of the main text. The BSs are then given by $\hat{B}(\cos^{-1}1/\sqrt{\frac{N}{2}-n})$, where n is the number of BSs between the EBS and the BS in question. For $N=4$ and $N=6$ and $N=8$, mode output 2 is swapped with mode output $N-1$. For $N=8$, an additional swap of output modes 4 and 5 is made. For odd numbered mode bases ($N = 3, 5, 7$) the method is the same with the following modifications. The EBS has its reflectivity changed to $r = \frac{1}{2} - \frac{1}{2N}$. (See for example references [1, 2] for more details on $N = 3$). The vacua are mixed using beamsplitters as above, with one output arm having one less vacuum input. π phase shifts are applied to all BS outputs on the left of the EBS except for the one left output exiting the last BS. Mode outputs 1 and $N-1$ are swapped, and the network for $N=7$ has an additional swap between output modes 3 and 4. The homodyne gains g_i are optimised using

a genetic algorithm in order to maximally satisfy the van Loock-Furusawa inequalities. These gains g_i scale the contributions of the quadrature variances and are not to be confused with the electronic gains $e l_p$ used to adjust the MPHD photocurrents. Here, optimal homodyne gains are calculated using two measures: minimising the mean of the $N - 1$ inequalities; and minimising the variance of the set of inequalities. A trade-off between the two measures is needed, and preference is given to minimising the mean of the inequalities.

Inseparability

Supplementary Figure 1 shows the degree of inseparability we would obtain with different input squeezing levels of the two modes. The other $N-2$ modes are always vacua. Entanglement holds for any moderate squeezing levels, however the strength of inseparability becomes extremely weak, as we approach $N=50$.

Materials and methods

We use a dual-wavelength continuous-wave Nd:YAG laser at 1064 nm and 532 nm. The optical parametric amplifiers (OPA) each contain a periodically poled KTP crystal in a bow-tie cavity. The squeezed beams are almost identical in purity, with squeezing levels of approximately -6 dB and anti-squeezing of 8.5 dB. The beam containing the 8 spatially orthogonal modes (see main text) is made highly elliptical in order to be measured by the MPHD, which has a linear array of 8 photodiodes. The photodiode array used is a Hamamatsu InGaAs PIN photodiode array (G7150) which actually has 16 photodiodes however we choose to use only 8 of these in the present experiment.

Cluster State Computation

Cluster state computation utilizes the entangled cluster state as the resource basis for computation. Being a measurement based protocol, modifications are needed to increase the degrees of freedom in our detection scheme. The modifications needed are as follows. First, we need to introduce the ability to measure each mode in an arbitrary phase quadrature at the MPHD. This may be achieved by manipulating the phases between the copropagating modes. By introducing a unitary mode shaping device such as that explained in references [3, 4], such access to individual phases becomes possible. Second, measurement results of arbitrary cluster nodes require feed-forward to remaining cluster nodes. This may be implemented by combining a displacement beam containing the necessary phase space displacements with the beam containing the co-propagating mode to be displaced. The key point here is that the displacement beam would necessarily be shaped in order to interfere

with only one mode, utilizing the orthogonal nature of the spatial modes. Detailed analysis can be found in Morizur's PhD thesis [5].

[1] Aoki, T. et al. Experimental creation of a fully inseparable tripartite continuous-variable state. *Phys. Rev. Lett.* **91**

(**8**), 080404-1 (2003).

- [2] Braunstein, S. L. Quantum error correction for communication with linear optics. *Nature* **394**, 47 (1998).
- [3] Morizur, J-F. et al. Programmable unitary spatial mode manipulation. *JOSA A* **27**, **11** 2524-2531 (2010).
- [4] Morizur, J-F., Armstrong, S., Treppe, N., Janousek, J., Bachor, H-A. Spatial reshaping of a squeezed state of light. *EPJD* **61**, 1 237-239 (2011).
- [5] Morizur, J-F. *Quantum Protocols with Transverse Spatial Modes*. (PhD thesis, Aust. Nat. Univ., 2011).

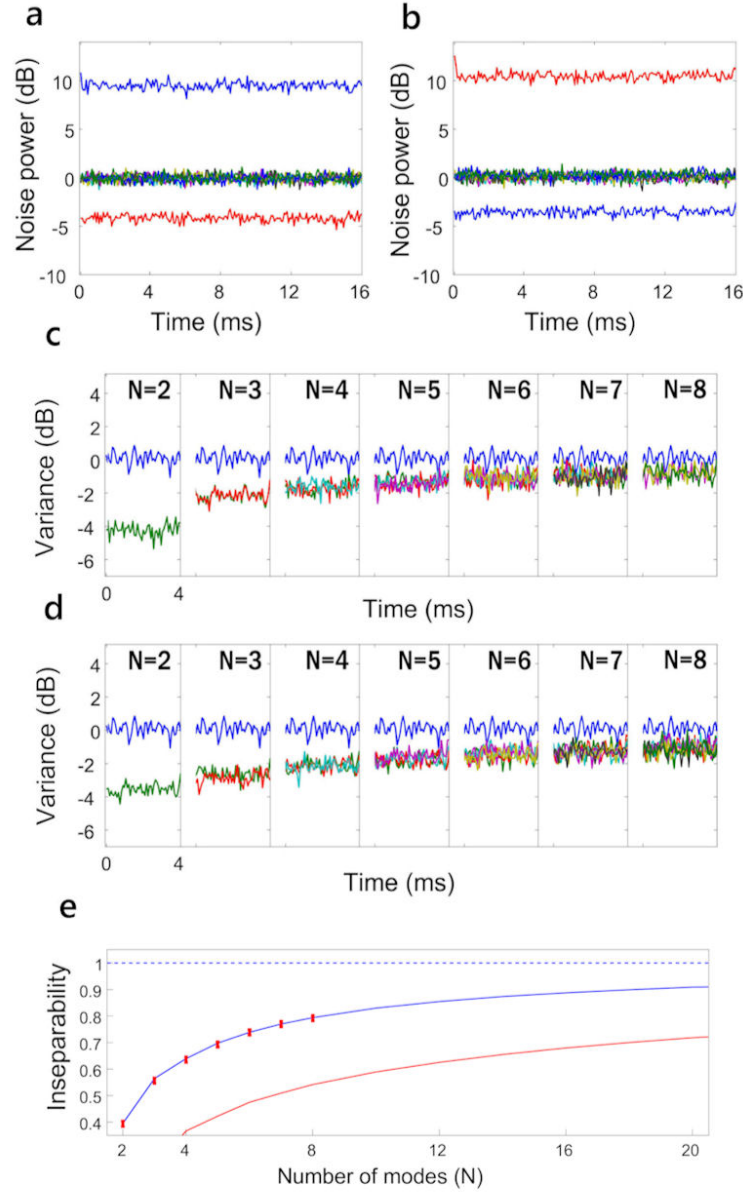


FIG. 4: Noise variance measurements of the spatial modes. **a**, x quadrature measurements of the input mode basis. The squeezed $\langle[\Delta x_1]^2\rangle$ is shown in the red and anti-squeezed $\langle[\Delta x_2]^2\rangle$ is shown in the blue. The x quadrature variances of the 6 vacua modes are measured to equal quantum noise (0dB). **b**, p quadrature measurements. The anti-squeezed $\langle[\Delta p_1]^2\rangle$ is shown in the red and squeezed $\langle[\Delta p_2]^2\rangle$ is shown in the blue. The p quadrature variances of the 6 modes are again measured to equal quantum noise, confirming they are vacua. **c**, These variances show the x quadrature correlations between modes as in the first half of the L.H.S. of equation (2) of the text. Every column shows N-1 traces of x quadrature correlations below shot noise, as well as the blue shot noise trace (0dB) normalised to two units of vacua. Each green trace shows $\langle[\Delta(\hat{x}_1^N - \hat{x}_2^N)]^2\rangle$ for each N-mode basis. Each new color represents the other N-1 variance correlation traces of equation (2). **d**, Correlations between measured modes in p quadrature, second half of the L.H.S. of equation (2). Each green trace now shows $\langle[\Delta(\hat{p}_1^N + \hat{p}_2^N + g_3\hat{p}_3^N + \dots + g_N\hat{p}_N^N)]^2\rangle$. The traces overlapping shows that each pair of modes is entangled with the same strength as any other pair of modes, a result of optimising for symmetry in the virtual networks. **e**, The blue dashed line represents the bound of separability. The red rectangles are the measured experimental values given by adding together the x quadrature correlation terms and the p quadrature correlation terms (L.H.S. of equation 2). The blue line (theory) shows inseparability as a function of the number of modes in the basis, with the same two squeezed inputs used in the experiment. All experimental losses have been taken into account. The red line (theory) predicts the degree of inseparability given two symmetric squeezed inputs of -10dB each, and again N-2 vacua. Refer to the supplementary material for how the networks are constructed.

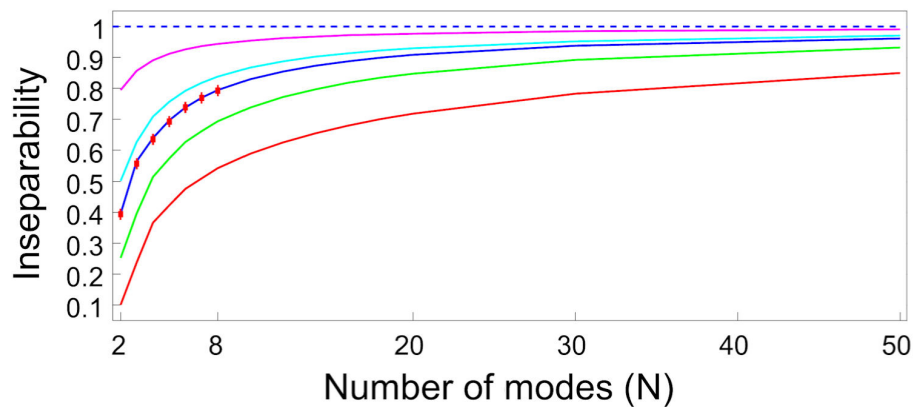


FIG. 5: Inseparability for different squeezed inputs. The blue dashed line represents the bound of separability. All traces have two squeezed inputs and $N-2$ vacua modes, as in the experiment. What changes is the amount of squeezing in the two squeezed inputs, assumed here to be symmetric with equal anti-squeezing. From the top we have: -1dB (magenta); -3dB (cyan); experimental parameters (blue); experimental values (red rectangles); -6dB (green); and -10dB (red).